Available online at www.sciencedirect.com
ScienceDirect
Trans. Nonferrous Met. Soc. China 27(2017) 1248−1256
Transactions of Nonferrous Metals Society of China
www.tnmsc.cn

Processing map and microstructure evaluation of AA6061/Al_2O_3 nanocomposite at different temperatures

H. R. EZATPOUR[1], S. A. SAJJADI[2], M. HADDAD SABZEVAR[2], A. CHAICHI[3], G. R. EBRAHIMI[4]

1. Faculty of Engineering, Sabzevar University of New Technology, Sabzevar 9615131113, Iran;
2. Department of Materials Science and Metallurgical Engineering, Engineering Faculty, Ferdowsi University of Mashhad, Mashhad, Iran;
3. Department of Mechanical & Industrial Engineering, Louisiana State University, Baton Rouge, Louisiana 70803, USA;
4. Department of Materials and Polymer Engineering, Hakim Sabzevari University, Sabzevar, Iran

Received 20 May 2016; accepted 12 September 2016

Abstract: Hot compression behavior of Al6061/Al_2O_3 nanocomposite was investigated in the temperature range of 350−500 °C and the strain rate range of 0.0005−0.5 s^{-1}, in order to determine the optimum conditions for the hot workability of nanocomposite. The activation energy of 285 kJ/mol for the hot compression test is obtained by using hyperbolic sine function. By means of dynamic material model (DMM) and the corresponding processing map, safe zone for the hot workability of AA6061/Al_2O_3 is recognized at temperature of 450 °C and strain rate of 0.0005 s^{-1} and at temperature of 500 °C and the strain rate range of 0.0005−0.5 s^{-1}, with the maximum power dissipation efficiency of 38%. Elongated and kinked grains are observed at 400 °C and strain rate of 0.5 s^{-1} due to the severe deformation.

Key words: nanocomposite; hot compression test; processing map; dynamic recrystallization; instability flow

1 Introduction

Metal matrix composites (MMCs) have been an amazing subject during the past decades and aluminum alloys have assumed the most attractive title in this sphere [1−3]. Not only because of their low density and high specific strength, but also due to the incredible ability for strengthening by reinforcement particles, many researchers endeavored to develop aluminum alloy properties either in the experimental scale or for industrial purposes [4,5]. Furthermore, the costs of production and manufacturing of aluminum metal matrix composites (AMMCs) are much more affordable and reasonable in comparison with other lightweight metals such as magnesium and titanium alloys [6,7]. Accordingly, there are a wide volume of applications which are undoubtedly dependent on the enhancement of this sort of alloy, particularly in automotive and transport industries [7,8].

Metal matrix composites (MMCs) that comprise a uniform dispersion of reinforcements in the size range of nanometers are defined as metal matrix nanocomposites (MMNCs) [9,10]. MMNCs are the predominant materials for the future of several applications because of their capacity in the improvement of toughness and ductility, which are the most challenging disadvantages of MMCs [6,8,9]. By decreasing the size of reinforcement particles, it is very likely to achieve a finer grain microstructure due to the suppression of grain growth during solidification stage which can result in the enhancement of mechanical properties [11−13]. Meanwhile, the trapping of air and formation of bubbles increase with reduction of the size of particles, which dramatically decrease the mechanical properties of composite [9]. Therefore, substituting micro ceramic particles with nanoparticle reinforcements is also accompanied with some challenges [14].

AA6061 alloy, a precipitation hardened aluminum alloy, in which magnesium and silicon are the fundamental alloying elements [15,16], exhibits unique welding, extrusion and forging abilities, and it is considered as one of the most widely used aluminum alloys for the construction of automotive parts such as

Corresponding author: H. R. EZATPOUR; Tel/Fax: +98-5144200750; E-mail: H.R.Ezatpour@gmail.com
DOI: 10.1016/S1003-6326(17)60145-6

wheel spacer [17,18]. Many studies have been conducted in order to reinforce AA6061 matrix by silicon carbide [19], aluminum oxide [15,20−24] and zirconia [25], and aluminum oxide is considered as the most compatible ceramic reinforcement for aluminum matrix composites [15]. Moreover, it is reported [26] that the application of aluminum matrix composites has been improved to 1000 °C due to the high melting point of Al_2O_3 and its remarkable compatibility with the matrix. It is noteworthy to indicate that the bonding of ceramic particles through the matrix can be improved by reducing the interface between particles and matrix [9,27].

Hot deformation is a process, in which the work piece is deformed plastically above its recrystallization temperature [21,28]. The recrystallization phenomenon can result in the increase of ductility while strain hardening process has decreased [29]. Predicting the appropriate temperature range and strain rate is necessary by investigating the alternation of large plastic flow irreversible thermodynamics for a prosperous isotherm forging of metals and MMCs [30]. Dynamic material model (DMM) is a thermodynamic approach based means for obtaining the optimal conditions of hot deformation process [30]. Dissipated and stored energies in the work piece are two fundamental criteria in this model in order to assess the microstructural evolutions [31]. According to Eq. (1), the overall power (P) received by the specimen is divided into two distinct terms, where G is the value of energy dissipated by the plastic deformation and J demonstrates the role of other metallurgical mechanisms, also σ and $\dot{\varepsilon}$ are defined as the instantaneous stress and strain rate, respectively [21].

$$P=\sigma\dot{\varepsilon}=G+J=\int_0^{\dot{\varepsilon}}\sigma \mathrm{d}\dot{\varepsilon}+\int_0^{\sigma}\dot{\varepsilon}\mathrm{d}\sigma \quad (1)$$

SPIGARELLI et al [21] investigated the hot workability of AA6061 reinforced by micro particles of Al_2O_3 by constitutive equations. They have considered the climb of dislocations as the major mechanism for controlling the hot deformation behavior of this alloy. Furthermore, FAN et al [32] studied the hot deformation of AA6061 by uniaxial compression tests in the temperature range of 400−500 °C and strain rate of 0.01−1 s^{-1}. Their results consider dynamic recovery (DRV) and dynamic recrystallization (DRX) as the main mechanisms for hot deformation at high temperatures [32]. Dynamic precipitation is also observed at 400 °C and it has been considerably dependent on the variation of temperature [32]. MROWKA-NOWOTNIK et al [33] reported that the stress level reduced with the increase of temperature and decreasing strain rate, and the activation energy of deformation process was noticeably dependent on the process parameters. Moreover, they also mentioned DRV and DRX mechanisms as the ruling factors for dynamic flow softening [33]. However, there is still no report concerning the characterization of AA6061/Al_2O_3 nanocomposite hot workability. Moreover, previous researches in the field of hot deformation process of aluminum-based nanocomposites, microstructural evolutions and a comprehensive connection between optimal hot deformation parameters and microstructural observations were insufficient. Hence, investigation with more details is necessary to clarify the microstructure evolutions during hot deformation of aluminum metal matrix nanocomposites and develop optimal conditions for hot workability of such materials [34].

In the current study, AA6061/0.5%Al_2O_3 nanocomposite was produced by stir casting method and extruded as a secondary process for the improvement of mechanical properties. Hot deformation behavior of AA6061/Al_2O_3 nanocomposite was investigated in the temperature range and strain rate range of 350−500 °C and 0.0005−0.5 s^{-1}, sequentially. Hot deformation data and microscopic observations were used to determine the optimal conditions for hot working of nanocomposite in a practical manner.

2 Experimental

Aluminum oxide (Al_2O_3) nanoparticles were prepared by Merck Company with the mean size of 40 nm and used as the reinforcement additive. The metal matrix consists of 0.65% Si, 0.7% Fe, 0.25% Cu, 0.15% Mn, 0.9% Mg, 0.07% Cr, 0.25% Zn, 0.15% Ti, and balance aluminum.

A combination of stir casting and extrusion procedure was employed for the production process. Firstly, the amount of 0.5% nanoparticles were injected through the molten aluminum by the pressure of pure argon gas at 750 °C for 20 min followed by a 15 min extra stirring in order to achieve a more homogenized mixture. The stirring speed was 450 r/min. Afterwards, a solution heat treatment was performed at 550 °C for 2 h on the manufactured bars prior to the extrusion process. The extrusion ratio η (η=$(D_0/D_1)^2$) was chosen as 2.8, where D_0 is the initial diameter and D_1 is the final diameter. High magnification SEM micrograph of nanocomposite is shown in Fig. 1.

All the samples, for the hot compression studies, were machined by automatic cutting device with height and diameter of 15 mm and 10 mm, respectively. Subsequently, a T6 heat treatment was accomplished after the extrusion with solution temperature and time of 550 °C and 2 h, while age hardening temperature and time were 200 °C and 3 h, respectively.

Hot workability of samples were investigated by

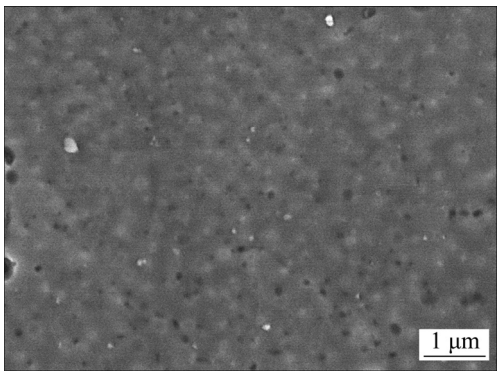

Fig. 1 High magnification SEM micrograph of Al6061/0.5% Al_2O_3 nanocomposite

Santam 1500 thermo mechanical simulator at the temperature of 350−500 °C and the strain rate of 0.0005−0.5 s^{-1}. Temperature measurements were done by a touching thermocouple located on the surface of the samples. The hot working temperature was selected by recrystallization temperature and the common hot working temperatures for aluminum alloys. Strain rate range was selected based on hot forming process of aluminum alloys in industry. After compression test, specimens were quenched rapidly in water. Mica sheet was used as lubricant to minimize friction between holder and workpiece. For microscopic studies, all the deformed specimens were prepared by gridding on 800, 1000, 2000 and 3000 grit papers. High resolution transmission electron microscopy (HRTEM), scanning electron microscopy (SEM: Mode Secondary electron, Volt: 5 kV) and optical microscopy (LM) were employed for observation the microstructural evolutions and hot deformation behavior of nanocomposite.

3 Results and discussion

3.1 Stress−strain curves and constitutive equation

Figure 2 demonstrates the flow curves of AA6061/Al_2O_3 nanocomposite. All the diagrams were delineated in the temperature range of 350−500 °C and strain rate range of 0.0005−0.5 s^{-1}. As is evident, the curves develop rapidly and reach a maximum at low strains during the high temperature and low strain rate. Afterwards, the diagrams maintain a constant and stable flow stress continuously. The fundamental justification for the increment of flow stress at low strains is the work hardening mechanism that causes an increase in the inception and then is suppressed by softening phenomena. At high temperatures, softening mechanisms such as DRX and DRV reduce the density of dislocations in order to decrease work hardening. Therefore, strain

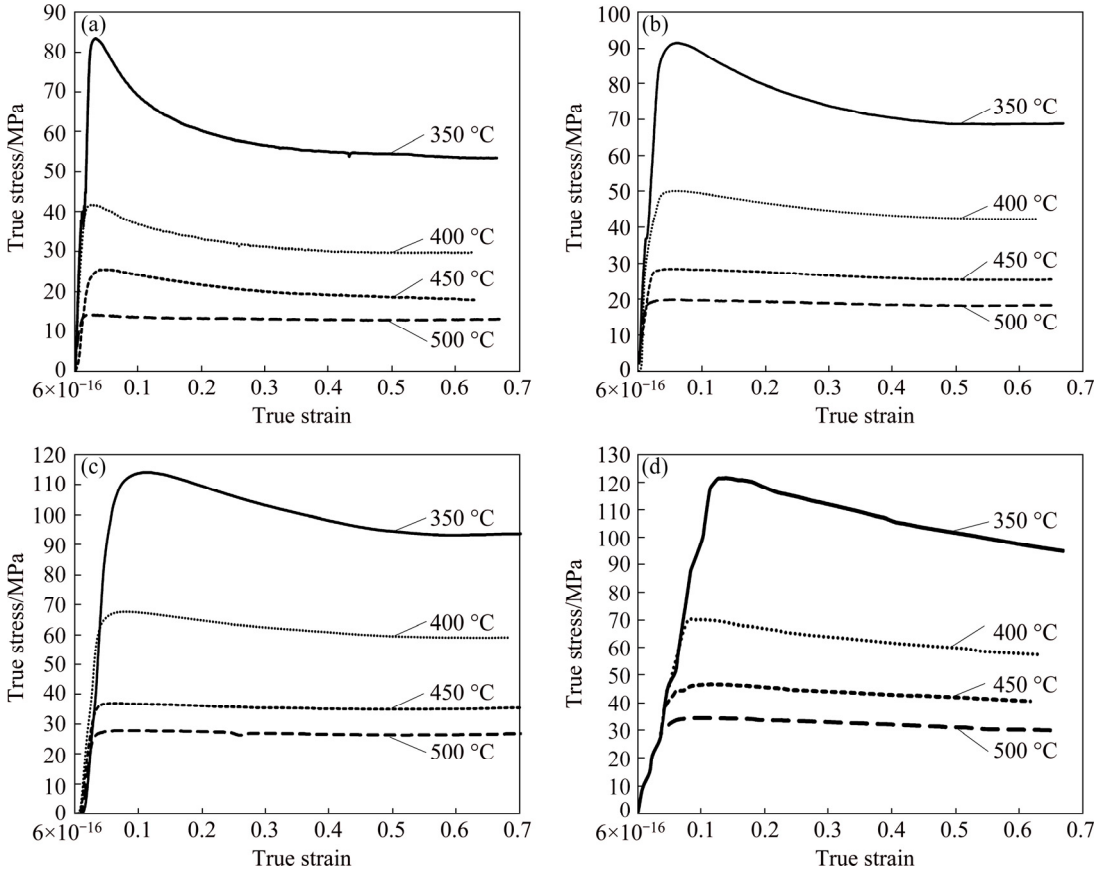

Fig. 2 Stress−strain flow curves of AA6061/Al_2O_3 nanocomposite in temperature range of 350−500 °C and strain rates of 0.0005 s^{-1} (a), 0.005 s^{-1} (b), 0.05 s^{-1} (c) and 0.5 s^{-1} (d)

hardening mechanisms disappear gradually until both of the softening and hardening phenomena acquire a steady state regime. In this case, dislocations possess higher capability of climbing and sliding at high temperatures and low strain rates due to the sufficient time for diffusion [35,36].

For metals and alloys with low or medium stacking fault energy, the material undergoes a critical microstructural condition which is accompanied with the lowering work hardening rate or nucleation of new grains. That starts when strain reaches a critical point. The critical strain (ε_c) can be measured by drawing the variation of strain hardening rate ($d\theta$=$d\sigma/d\varepsilon$) via the strain during hot deformation process [37]. As can be seen in Fig. 3, by increasing the temperature (or decreasing the strain rate), the critical strain decreases. Figure 4 presents the variation of peak stress as a function of temperature at different strain rates for the nanocomposite. As is evident, the amount of peak stress diminishes gradually by increasing the temperature in the range of 350−500 °C and decreasing strain rate from 0.5 s^{-1} to 0.0005 s^{-1}. With increasing the temperature or decreasing the strain rate, the diffusion rate of the atoms (D) increases. Therefore, the dislocation climb as well as slip is easier and the tendency for activation of work softening mechanisms and the migration of grain boundaries increase during hot deformation.

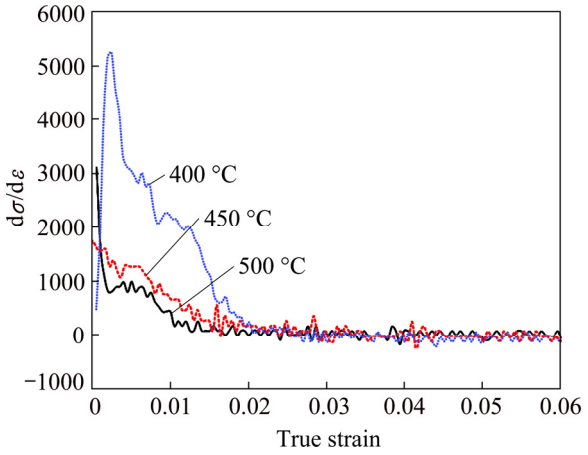

Fig. 3 Variation of $d\sigma/d\varepsilon$ vs strain (ε) at different temperatures and strain rate of 0.0005 s^{-1}

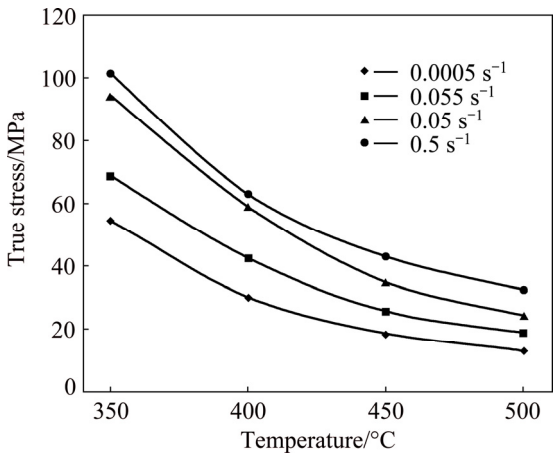

Fig. 4 Variation of peak stress (σ) vs temperature in strain rate range of 0.0005−0.5 s^{-1}

To employ the Zener−Holloman parameter ($Z=\dot{\varepsilon}\exp[-Q/(RT)]$), the relationship among temperature, strain rate and stress is clarified for nanocomposite by Eq. (2) [31,35]:

$$\lg\dot{\varepsilon}=n[\lg\sinh(\alpha\sigma)]\left(\frac{-Q}{RT}\right)+\lg A \quad (2)$$

The activation energy (Q) is obtained by Eq. (3) [3]:

$$Q=2.3RnS \quad (3)$$

where n and S are defined as the slope of $\ln\dot{\varepsilon}$ as a function of $\lg\sinh(\alpha\sigma)$ and slope of $\lg\sinh(\alpha\sigma)$ as a function of absolute temperature at different strain rates, sequentially. Moreover, α parameter is defined as a constant. The diagrams are demonstrated in Fig. 5 for the nanocomposite.

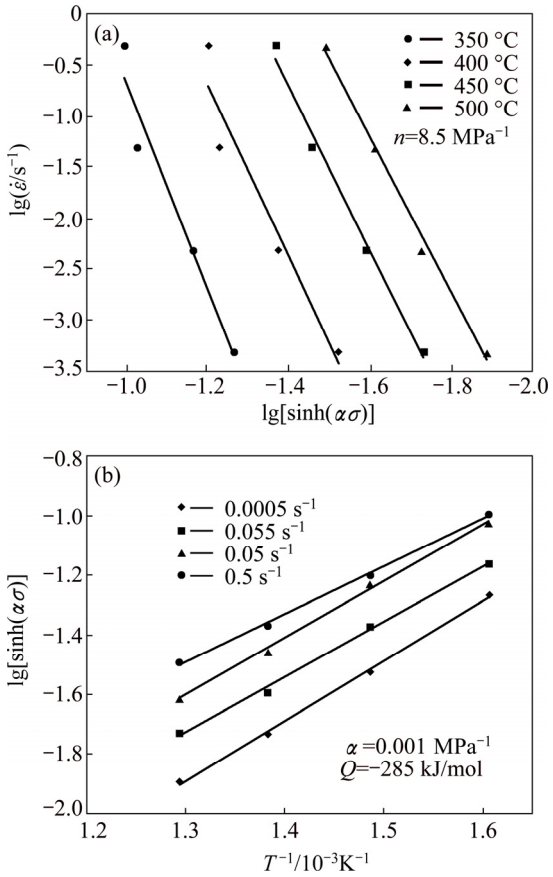

Fig. 5 Logarithmic plot of strain rate vs $\sinh(\alpha\sigma)$ (a) and $\sinh(\alpha\sigma)$ vs absolute temperature (b) of Al6061/Al_2O_3 nanocomposite

The values of Q and other constants are represented in Table 1. At last, the general equation for hot deformation of AA6061/Al_2O_3 nanocomposite is shown as

$$\dot{\varepsilon} = 8.6\times10^{15}[\sinh(0.001\sigma)]^{8.5}\exp\left(\frac{-285000}{RT}\right) \quad (4)$$

As reported in Table 1, the activation energy for AA6061/Al_2O_3 nanocomposite is 285 kJ/mol that is higher than that obtained for hot deformation of AA6061 (274 kJ/mol) [36]. This increment resulted from the addition of ceramic nanoparticles. It is reported by other researchers that ceramic nanoparticles would be able to postpone the occurrence of softening mechanisms by hindering the growth of either grain boundaries or sub-grains [12,30]. SENTHILKUMAR et al [30] studied the influence of TiC nanoparticles as the reinforcement additive for Al5083 alloy, and they concluded that the amount of activation energy increased by 30% in comparison with the base alloy. Another research was conducted by EZATPOUR et al [3] and the amount of Q for hot deformation process of AA7075 alloy increased from 196 kJ/mol to 227 kJ/mol because of the addition of alumina nanoparticles. This theory is supported by the fact that in metals with medium stacking fault energy, reinforcement nanoparticles act as a barrier and prevent the movement of dislocations and grain boundaries while stabilize the microstructure of matrix and diminish the tendency of matrix for the activation of softening mechanisms [31].

Table 1 Activation energy and other constants of AA6061/Al_2O_3 nanocomposite

A/s^{-1}	α/MPa^{-1}	n	Q/(kJ·mol^{-1})
8.6×10^{15}	0.001	8.5	285

Table 2 indicates Z value at different temperatures and strain rates for AA6061/Al_2O_3 nanocomposite. Softening mechanisms play a crucial role in the variations of Z parameter in different circumstances. It is believed that the value of Z parameter decreases by rising the temperature and decreasing the strain rate due to the occurrence of softening mechanisms.

Table 2 Logarithm of Zener−Holloman parameter at different temperatures and strain rates

Strain rate/s^{-1}	lg Z			
	350 °C	400 °C	450 °C	500 °C
0.0005	20.6	18.8	17.3	15.9
0.005	21.6	19.8	18.3	16.9
0.05	22.6	20.8	19.3	17.9
0.5	23.6	21.8	20.3	18.9

Figure 6 confirms the linear correspondence between the Zener−Holloman parameter and hyperbolic sine equation, which depicts the validity of creep hyperbolic sine equation used for hot compression behavior of the nanocomposite.

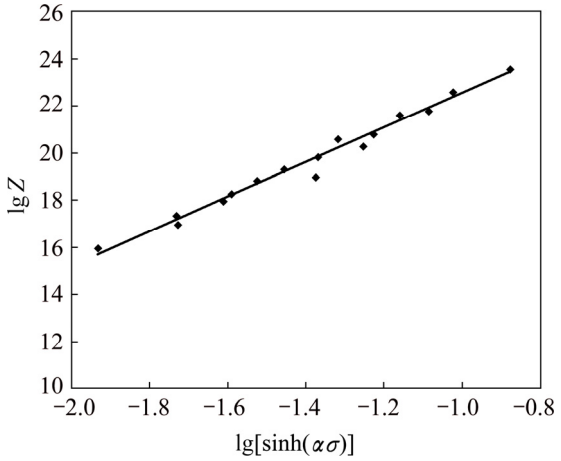

Fig. 6 Logarithmic plot of variation of Zener−Holloman parameter vs sinh($\alpha\sigma$) of Al6061/Al_2O_3 nanocomposite

3.2 Processing map

A prevalent approach for designation of optimal hot deformation circumstances is by achieving the processing map of the work piece [31,38]. In this method, the instability parameter (ξ) and the efficiency of power dissipation (η) are plotted into 2D maps as a function of $\ln\dot{\varepsilon}$ and absolute temperature for a specific amount of strain. The corresponding equations for the calculation of ξ and η are defined as Eq. (5) and Eq. (6) [38,39].

$$\xi\dot{\varepsilon} = \frac{\partial\ln\left[\frac{m}{m+1}\right]}{\partial\ln\dot{\varepsilon}} + m \quad (5)$$

$$\eta = \frac{J}{J_{\max}} \quad (6)$$

where J ($J = \frac{m\sigma\dot{\varepsilon}}{m+1}$) and m are power dissipation of the material and strain rate sensitivity parameter, respectively.

Unstable flow conditions are detected when the value of $\xi\dot{\varepsilon}$ is negative. The negative amount of $\xi\dot{\varepsilon}$ is unfavorable because of the occurrence of two common types of instabilities. The first one is the formation of adiabatic shear bands and flow localization that might lead to embellishment of a heterogeneous microstructure which is considerably deleterious for structural applications. The second type consists of different sorts of crack formation.

The processing map for AA6061/Al_2O_3 nanocomposite is drawn in Fig. 7 for the strain of 0.5. According to the processing map, the safe domain for hot workability of AA6061/Al_2O_3 is at temperature of 450 °C and strain rate of 0.0005 s^{-1} and at temperature of 500 °C and the strain rate range of 0.0005−0.5 s^{-1}. The maximum efficiency (η) is approximately 38%.

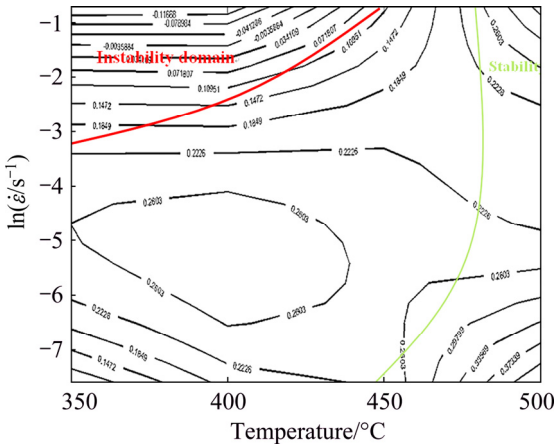

Fig. 7 Processing map of AA6061/Al_2O_3 nanocomposite

Meanwhile, the amount of power dissipation efficiency for AA6061 matrix is reported as 47% [36].

Hence, by the addition of ceramic nanoparticles, the efficiency of power dissipation decreases. Power dissipation capacity is generally controlled by the predominant mechanisms during the hot deformation process. Although for the aluminum matrix without any reinforcement, DRX phenomenon is a dominant factor, in case of the nanocomposite, DRV mechanism also plays a significant role which is reported by other researchers [20,33,40].

3.3 Microstructural evaluation

Optical microscopy observations are demonstrated in Fig. 8 for the deformed samples at the temperatures of 400−500 °C and strain rates of 0.0005 s^{-1} and 0.5 s^{-1}. Uniform elongated grains are explicitly observable at temperature of 400 °C and strain rate of 0.0005 s^{-1}; meanwhile there is no recrystallized grain in the microstructure (Fig. 8(a)). In the temperature range of 450−500 °C, DRX mechanism is activated while the new grains nucleate at previous grain boundaries. The size and number of recrystallized grains increase with the increase of temperature (Figs. 8(b)−(c))). At high temperature and low strain rate, grain boundary migration has an effective role in dynamic

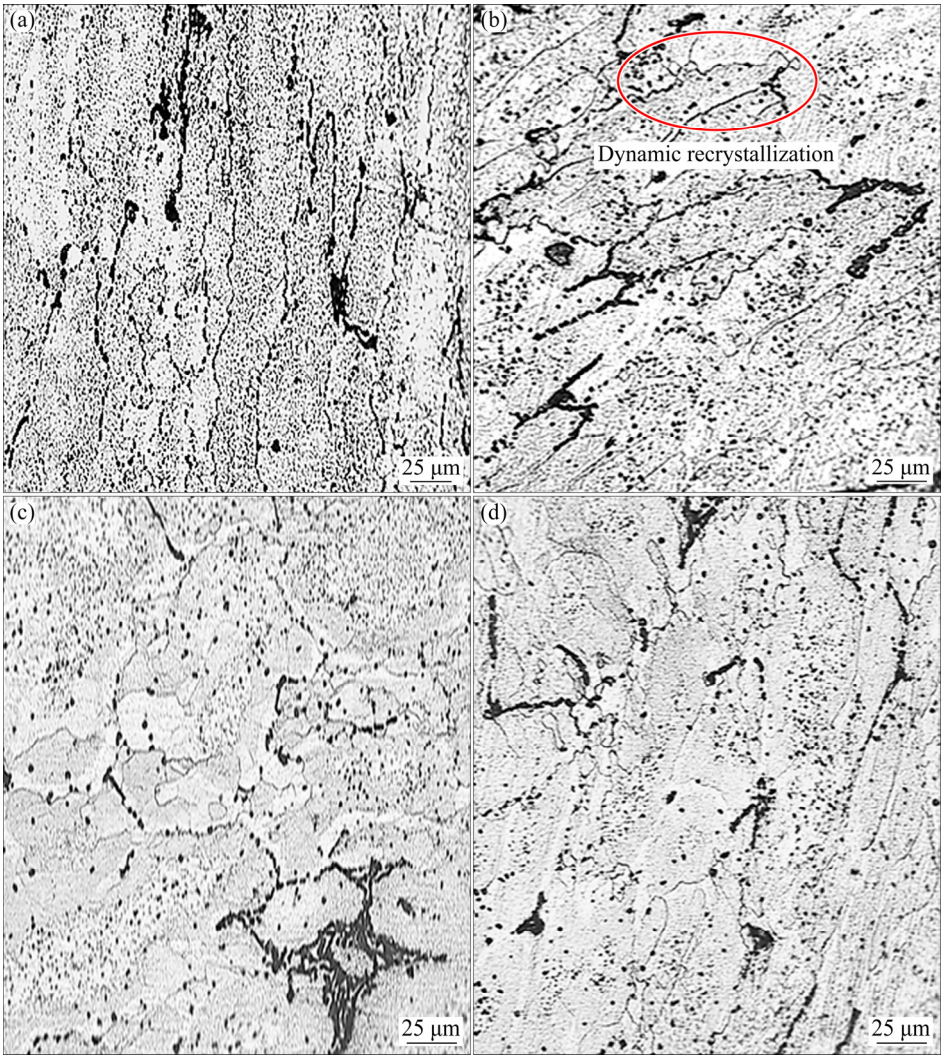

Fig. 8 Optical microscopy images of nanocomposite after hot deformation at strain rate of 0.0005 s^{-1} and different temperatures: (a) 400 °C; (b) 450 °C; (c) 500 °C; (d) 500 °C

recrystallization. Also, Fig. 8(d) shows recrystallized grains at high temperature and strain rate. At high strain rate, diffusion of atoms is limited, so the cross-sliding and climbing of dislocations have decreased and the density of dislocations has increased with resulting increment of stored energy in system. Consequently, the stored energy of the alloy reaches a critical value. As a result, work softening mechanisms such as DRV and DRX occur at high temperatures which decrease stored energy in system.

TEM images for AA6061/Al_2O_3 nanocomposite (Fig. 9) are shown at the temperature of 400−500 °C and strain rate of 0.0005 s^{-1}. As is evident, the density of dislocations is reduced with increasing the temperature from 400 to 500 °C.

According to the microstructure evaluations of AA6061 that is reported elsewhere [36], it is possible to compare the microstructural results of nanocomposite with the matrix. It is noteworthy to mention that the dynamic recrystallization is remarkably decreased by the addition of ceramic reinforcements to the aluminum matrix, and this fact has a considerable negative effect on the hot deformation behavior of nanocomposite. The existence of dispersed nanoparticle reinforcements suppresses the migration of grain boundaries by pinning as shown in Fig. 9(a). Therefore, the tendency of nanocomposite for activation of softening mechanisms dramatically decreases, which is tightly dependent on the migration of grain boundaries.

According to the processing map analysis and microstructure evaluations of the nanocomposite, unstable domain is determined at the temperature of 350−400 °C and strain rate of 0.5 s^{-1}. Figure 10 shows the flow instability of nanocomposite. Optical microstructure reveals the elongated and kinked grains at 400 °C and strain rate of 0.5 s^{-1}. Severe deformation is mostly considered as the main factor for the occurrence of kinked grain boundaries (Fig. 10(a)). Furthermore, SEM images confirm the shear banding growth due to the severe deformation and the presence of reinforcement particles in this region (Fig. 10(b)). The chance of adiabatic shear banding formation at high strain rates increases with the existence of nanoparticles due to the discrepancy between thermal conductivity of matrix and

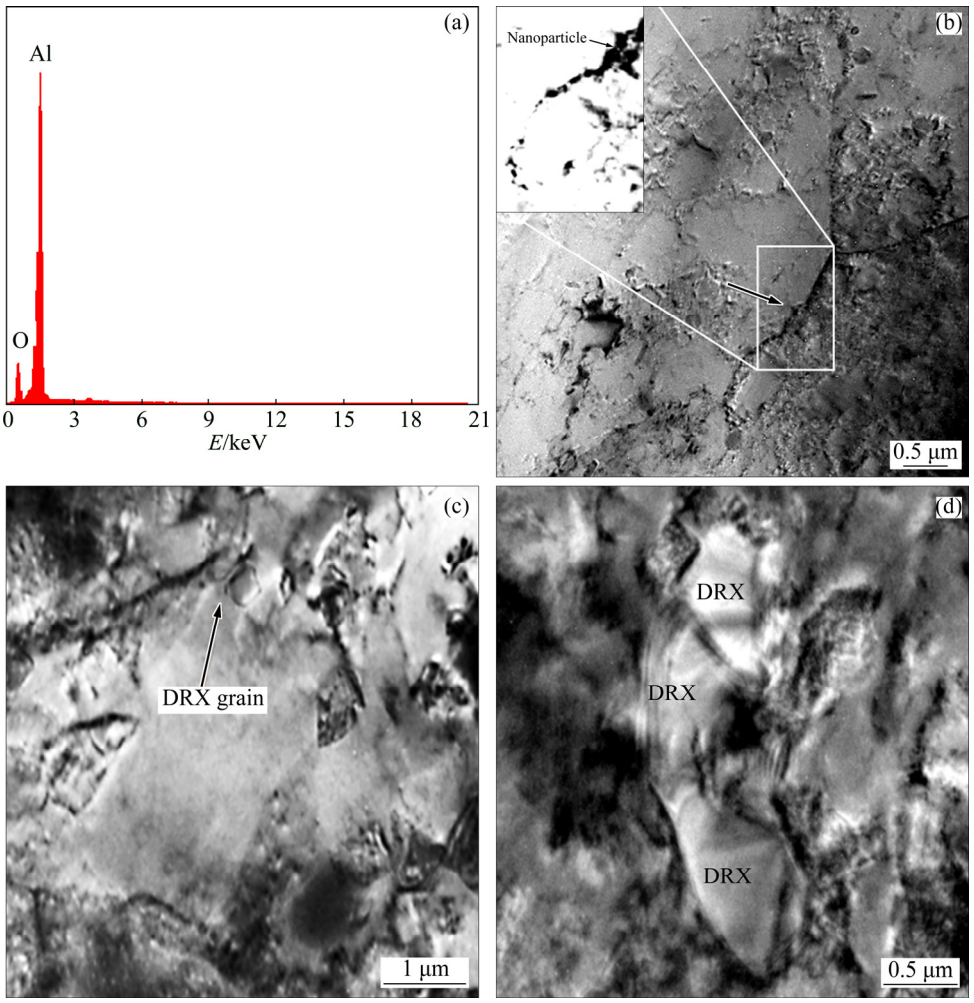

Fig. 9 TEM images of AA6061/Al_2O_3 nanocomposite after hot deformation at 400 °C (a), 450 °C (b), 500 °C (c), and strain rate of 0.0005 s^{-1}

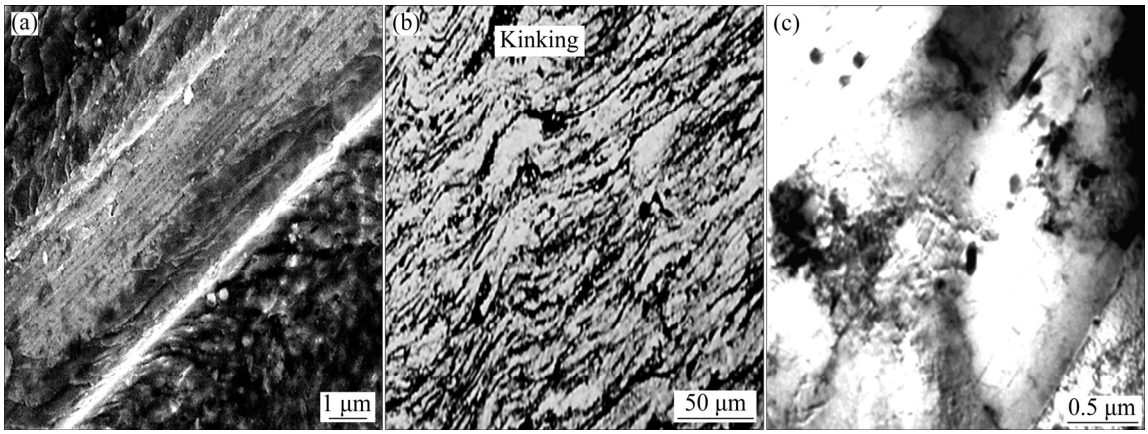

Fig. 10 SEM, OM and TEM images of AA6061/Al_2O_3 after hot deformation at temperature of 400 °C and strain rate of 0.5 s^{-1} (All of images illustrate flow instability by formation of kinked grains and shear bands)

reinforcement [41]. However, the deformed zone is supposed to be elongated in the unstable domain with the agreement of TEM images (Fig. 10(c)).

4 Conclusions

1) According to the stress−strain curves of the nanocomposite, the flow stress decreases with increasing the temperature and decreasing the strain rate due to the activation of work softening mechanisms.

2) The constitutive equation for AA6061/Al_2O_3 nanocomposite is

$$\dot{\varepsilon} = 8.6\times10^{15}[\sinh(0.001\sigma)]^{8.5}\exp\left(\frac{-285000}{RT}\right).$$

3) The optimum conditions for hot deformation of the nanocomposite were obtained at temperature of 450 °C and strain rate of 0.0005 s^{-1} and temperature of 500 °C and strain rate of 0.0005−0.5 s^{-1}.

4) Microscopic evaluations approve the occurrence of DRX as the work softening mechanism in nanocomposite.

5) Adiabatic shear banding and severe deformation are considered as the significant factors for the expansion of unstable zone.

References

[1] SURESH S. Fundamentals of metal-matrix composites [M]. Amsterdam: Elsevier Science, 2013.

[2] BHUSHAN R K, KUMAR S, DAS S. Fabrication and characterization of 7075 Al alloy reinforced with SiC particulates [J]. The International Journal of Advanced Manufacturing Technology, 2013, 65: 611−624.

[3] EZATPOUR H R, CHAICHI A, SAJJADI S A. The effect of Al_2O_3-nanoparticles as the reinforcement additive on the hot deformation behavior of 7075 aluminum alloy [J]. Materials & Design, 2015, 88: 1049−1056.

[4] SARAVANAN C, SUBRAMANIAN K, KRISHNAN V A, NARAYANAN R S. Effect of particulate reinforced aluminium metal matrix composite — A review [J]. Mechanics and Mechanical Engineering, 2015, 19: 23−30.

[5] HATCH J E, ASSOCIATION A. Aluminum: Properties and physical metallurgy [M]. Arlington: Aluminum Association Inc. and ASM International, 1984.

[6] CÖCEN Ü, ÖNEL K. Ductility and strength of extruded SiC_p/aluminium-alloy composites [J]. Composites Science and Technology, 2002, 62: 275−282.

[7] EVANS A, SAN MARCHI C, MORTENSEN A. Metal matrix composites in industry: An introduction and a survey [M]. New York: Springer Science & Business Media, 2013.

[8] GAY D. Composite materials: Design and applications [M]. UK: CRC Press, 2014.

[9] AJAYAN P M, SCHADLER L S, BRAUN P V. Nanocomposite science and technology [M]. New York: John Wiley & Sons, 2006.

[10] SALEHI M, SAADATMAND M, AGHAZADEH MOHANDESI J. Optimization of process parameters for producing AA6061/SiC nanocomposites by friction stir processing [J]. Transactions of Nonferrous Metals Society of China, 2012, 22(5): 1055−1063.

[11] BAYRAKTAR E, ROBERT M H, MISKIOGLU I, BAYRAKTAR A T. Mechanical and tribological performance of aluminium matrix composite reinforced with nano iron oxide (Fe_3O_4) [J]. Composite, Hybrid, and Multifunctional Materials, 2015, 4: 185−192.

[12] CASATI R, VEDANI M. Metal matrix composites reinforced by nano-particles—A review [J]. Metals, 2014, 4: 65−83.

[13] SABERI Y, ZEBARJAD S, AKBARI G. On the role of nano-size SiC on lattice strain and grain size of Al/SiC nanocomposite [J]. Journal of Alloys and Compounds. 2009, 484: 637−640.

[14] BAHRAMI M, DEHGHANI K, GIVI M K B. A novel approach to develop aluminum matrix nano-composite employing friction stir welding technique [J]. Materials & Design, 2014, 53: 217−225.

[15] EKAMBARAM S, MURUGAN N. Synthesis and characterization of aluminium alloy AA6061-alumina metal matrix composite [J]. International Journal of Current Engineering and Technology, 2015, 5: 3211.

[16] METZGER G. Some mechanical properties of welds in 6061 aluminum alloy sheet (Aluminum alloy sheet welds with high silicon and magnesium content analyzed for tensile properties and fracture toughness) [J]. Welding Journal, 1967: 46: 457−469.

[17] OZTURK F, SISMAN A, TOROS S, KILIC S, PICU R. Influence of aging treatment on mechanical properties of 6061 aluminum alloy [J]. Materials & Design, 2010, 31: 972−975.

[18] GLADSTON J, SHERIFF N, DINAHARAN I, RAJA SELVAM J. Production and characterization of rich husk ash particulate reinforced AA6061 aluminum alloy composites by compocasting [J].

Transactions of Nonferrous Metals Society of China, 2015, 25(3): 683−691.
[19] JAYASHREE P, SHANKAR M G, KINI A U, SHARMA S, SHETTY R. Review on effect of silicon carbide (SiC) on stir cast aluminium metal matrix composites [J]. International Journal of Current Engineering and Technology, 2013, 3: 1061−1071.
[20] CERRI E, SPIGARELLI S, EVANGELISTA E, CAVALIERE P. Hot deformation and processing maps of a particulate-reinforced 6061+ 20% Al_2O_3 composite [J]. Materials Science and Engineering A, 2002, 324: 157−161.
[21] SPIGARELLI S, EVANGELISTA E, CERRI E, LANGDON T. Constitutive equations for hot deformation of an Al-6061/20% Al_2O_3 composite [J]. Materials Science and Engineering A, 2001, 319: 721−725.
[22] KWON Y, LEE Y, LEE J. Deformation behavior of Al−Mg−Si alloy at the elevated temperature [J]. Materials Processing Technology, 2007, 187−188: 533−536.
[23] DUAN Y. Hot deformation and processing map of Pb−Mg−10Al−1B alloy [J]. Materials Engineering and Performance, 2013, 22(10): 3049−3054.
[24] KANG C, KIM N, KIM B. The effect of die shape on the hot extrudability and mechanical properties of 6061 Al/Al_2O_3 composites [J]. Journal of Materials Processing Technology, 2000, 100: 53−62.
[25] LEWIS C, STOBBS W, WITHERS P. Internal stress induced debonding in a zirconia-reinforced 6061 aluminium alloy composite [J]. Materials Science and Engineering A, 1993, 171: 1−11.
[26] SAJJADI S A, PARIZI TORABI M, EZATPOUR H R, SEDGHI A. Fabrication of A356 composite reinforced with micro and nano Al_2O_3 particles by a developed compocasting method and study of its properties [J]. Journal of Alloys and Compounds, 2012, 511: 226−2231.
[27] EZATPOUR H R, SAJJADI S A. Microstructure and mechanical properties of Al/Al_2O_3 micro and nano nanocomposites fabricated by a novel stir casting [C]//Proceedings of the 2nd Conferences on Applications of Nano Technologie in Sciences, Engineering and Medicines-NTC, Iran: Azad Mashhad University, 2011.
[28] EVANGELISTA E, FORCELLESE A, GABRIELLI F, MENGUCCI P. Hot formability of AA 6061 PM aluminium alloy [J]. Materials Processing Technology, 1990, 24: 323−332.
[29] RAJAMUTHAMILSELVAN M, RAMANATHAN S. Hot deformation behaviour of 7075 alloy [J]. Journal of Alloys and Compounds, 2011, 509: 948−952.
[30] SENTHILKUMAR V, BALAJI A, NARAYANASAMY R. Analysis of hot deformation behavior of Al 5083-TiC nanocomposite using constitutive and dynamic material models [J]. Materials & Design, 2012, 37: 102−110.
[31] AHAMED H, SENTHILKUMAR V. Hot deformation behavior of mechanically alloyed Al6063/0.75Al_2O_3/0.75Y_2O_3 nano-composite—A study using constitutive modeling and processing map [J]. Materials Science and Engineering A, 2012, 539: 349−359.
[32] FAN X, LI M, LI D, SHAO Y, ZHANG S, PENG Y. Dynamic recrystallisation and dynamic precipitation in AA6061 aluminium alloy during hot deformation [J]. Materials Science and Technology, 2014, 30: 1263−1272.
[33] MRÓWKA-NOWOTNIK G, SIENIAWSKI J, KOTOWSKI S, NOWOTNIK A, MOTYKA M. Hot deformation of 6xxx series aluminium alloys [J]. Archives of Metallurgy and Materials, 2015, 60: 1079−1084.
[34] ENGLER OHIRSCH J. Texture control by thermomechanical processing of AA6xxx Al−Mg−Si sheet alloys for automotive applications—A review [J]. Materials Science and Engineering A, 2002, 336(1−2): 249−262.
[35] LI X, LIU C, LUO K, MA M, LIU R. Hot deformation behaviour of SiC/AA6061 composites prepared by spark plasma sintering [J]. Journal of Materials Science & Technology, 2016, 32: 291−297.
[36] EZATPOUR H, SABZEVAR M H, SAJJADI S A, HUANG Y. Investigation of work softening mechanisms and texture in a hot deformed 6061 aluminum alloy at high temperature [J]. Materials Science and Engineering A, 2014, 606: 240−247.
[37] JIN N, ZHANG H, HAN Y, WU W, CHEN J. Hot deformation behavior of 7150 aluminum alloy during compression at elevated temperature [J]. Materials Characterization, 2009, 60: 530−536.
[38] PRASAD Y. Processing maps: a status report [J]. Journal of Materials Engineering and Performance, 2003, 12: 638−645.
[39] JENAB A, TAHERI A K. Experimental investigation of the hot deformation behavior of AA7075: Development and comparison of flow localization parameter and dynamic material model processing maps [J]. International Journal of Mechanical Sciences, 2014, 78: 97−105.
[40] HAO S M, XIE J P, WANG A Q, WANG W Y, LI J W, SUN H L. Hot deformation behaviors of 35% SiC_p/2024Al metal matrix composites [J]. Transactions of Nonferrous Metals Society of China, 2014, 24: 2468−2474.
[41] DAVIS J. Metals handbook [M]. Ohio: ASM International, 1990.

不同温度下 AA6061/Al_2O_3 纳米复合材料的加工图和组织评价

H. R. EZATPOUR[1], S. A. SAJJADI[2], M. HADDAD SABZEVAR[2], A. CHAICHI[3], G. R. EBRAHIMI[4]

1. Faculty of Engineering, Sabzevar University of New Technology, Sabzevar 9615131113, Iran;
2. Department of Materials Science and Metallurgical Engineering, Engineering Faculty, Ferdowsi University of Mashhad, Mashhad, Iran;
3. Department of Mechanical & Industrial Engineering, Louisiana State University, Baton Rouge, Louisiana 70803, USA;
4. Department of Materials and Polymer Engineering, Hakim Sabzevari University, Sabzevar, Iran

摘　要：为确定热加工性能的最佳条件，在温度 350~500 °C、应变率 0.0005~0.5 s^{-1} 下研究 Al6061/Al_2O_3 纳米复合材料的热压缩行为。采用双曲正弦函数得到材料热压缩测试活化能为 285 kJ/mol。用动态材料模型和相应的加工图，确定了温度 450 °C、应变速率 0.0005 s^{-1} 和温度 500 °C、应变速率 0.0005~0.5 s^{-1} 为 Al6061/Al_2O_3 材料的热加工性能安全区，最大功率损耗率为 38%。由于材料大变形，在温度 400 °C 和应变速率 0.5 s^{-1} 下得到了被伸长和扭结晶粒。

关键词：纳米复合材料；热压缩测试；加工图；动态再结晶；流变失稳

(Edited by Xiang-qun LI)